PAPER

Assessment of paraffin removal from prostate FFPE sections using transmission mode FTIR-FPA imaging†

Caryn Hughes,[ab] Lydia Gaunt,[c] Michael Brown,[b] Noel W. Clarke[bde] and Peter Gardner*[ac]

Formalin-fixed paraffin-embedded (FFPE) tissue sections are routinely analysed for biochemical discrimination by vibrational spectroscopy techniques in the spectral pathology community. In these experiments, it is usually desirable to remove the paraffin from the tissue. This is most commonly performed by the use of xylene but other solvents such as hexane are also used. It is thought that the removal of unbound paraffin wax by such solvents also leaches out lipids native to the tissue, leading to the perception by some that any subsequent analysis on remaining lipids of dewaxed tissue may be unreliable. The scope of the study was to make an assessment of whether a dewaxing protocol can demonstrate that paraffin wax is reliably removed in relation to the detectable limits of transmission mode infrared spectroscopy. In this study, a specific sampling region of two serial FFPE sections of human prostate cancer were analysed by monitoring the methylene hydrocarbon-associated vibrations as a function of solvent immersion time during washes of either hexane or xylene. Results of the study indicate that after 5–10 minutes of immersion in the solvent the hydrocarbon-associated vibrations remain fairly consistent across the tissue. This suggests that while methylene chains of free, unbound tissue lipids are leached from the tissue (assumingly in the first tissue processing stages prior to paraffin embedding) solvent-resistant lipids remain present in formalin-fixed tissue due to being locked into protein–lipid complex matrices, predominantly in the membranes. It is these lipids signals that are subsequently detectable by spectral pathology and may still prove to be of diagnostic use.

1 Introduction

In standard histopathology, a wide variety of stains are utilised to aid disease-based detection during inspection of tissue morphology at a microscopic level. Spectral pathology, however, is a complementary, stain-free approach. Infrared spectroscopy is just one application of spectral pathology that can be used to probe the global biochemistry of the sample. When an infrared spectrometer is coupled to a microscope equipped with an appropriate detector, it is also possible to achieve spatially-resolved biochemical information.

Histology sample preparation for infrared spectroscopy is minimal and straight-forward. A tissue section, cut to a thickness of usually ~4–8 μm using a microtome, is floated onto an appropriate transparent substrate, such as calcium fluoride or barium fluoride. The sample can then be probed by spectroscopy. Choosing the method of initial sample preparation, however, is an issue. Ultimately, the more sample preparation that is performed before the sample is analysed, the less biologically relevant the biochemical signatures become.

Freezing tissue, for example, preserves the biochemistry without the use of solvents. The freezing processes however can cause damage; If the freezing process is too slow then ice crystals can form, puncturing cell membranes.[1,2] Additionally, the thawing processes in frozen tissue samples will cause a time-dependent sample degradation gradient. There are, however, a number good recommendations to avoid or inhibit these processes, as described by Stitt et al.[3]

Sometimes it is not possible to control the sample processing step. Retrospective investigation of diseased tissue often requires archived tissue from Bio-Banks where the favoured protocol may be formalin-fixed paraffin embedding (FFPE).

[a]Manchester Institute of Biotechnology, University of Manchester, 131 Princess Street, Manchester, M1 7DN, UK

[b]Genito Urinary Cancer Research Group, Institute for Cancer Sciences, Paterson Institute for Cancer Research, The University of Manchester, Manchester Academic Health Science Centre, The Christie NHS Foundation Trust, Manchester, M20 4BX, UK

[c]School of Chemical Engineering and Analytical Science, The University of Manchester, Oxford Road, Manchester, M13 9PL, UK

[d]Department of Urology, The Christie NHS Foundation Trust, Manchester, M20 4BX, UK

[e]Department of Urology, Salford Royal Hospital NHS Foundation Trust, Stott Lane, Salford, M6 8HD, UK

† Electronic supplementary information (ESI) available. See DOI: 10.1039/c3ay41308j

Fresh tissue is firstly immersed in an aqueous formalin solution, which acts as the fixative. The tissue is then dehydrated in washes of xylene and ethanol. Finally, an embedding medium of paraffin wax is added to the tissue, creating a protective barrier.

When the tissues are ready for spectroscopic analysis, efficient removal of paraffin wax is desired in order to probe the full biochemical range available. Digital dewaxing,[4] *i.e.* measuring the sample without physical dewaxing followed by digital removal of the paraffin absorption bands, is a possible option, but this is a further complication to spectral processing and it is yet to be seen how reliable the recovered lipid signals are after such a process. Doubt still remains, however, over the physical removal of paraffin during the dewaxing process and to what effect different solvents, such as hexane (C_6H_{14}) or xylene (C_8H_{10}), may contribute.[5,6]

A common worry is that by removing paraffin wax with hydrocarbon solvents we also run the risk of removing increasing proportions of the native residual hydrocarbons from the tissue. At the primary washing stage (before tissue is paraffin-embedded) unsaturated inherent hydrocarbons such as free unbound, free fatty acids and triglycerides are inevitably leached from the tissue; the presence of these lipid types can only be inferred by their absence in the form of unstained 'holes' that are left behind during staining.[7,8] To remove paraffin from the tissue prior to analysis, the same solvents are used to remove the large hydrocarbon chains of unbound paraffin wax. At this point any free unbound tissue lipids have already been removed from the tissue prior to paraffin embedding. The only tissue-related hydrocarbons that remain are the solvent-resistant type. There are a large variety of solvent-resistant lipids.[9] Those that are most resistant are the lipid components of complexes which are bound to tissue proteins during the process of formalin fixation, methylene bridges form between proteins. It is known that lipids, nucleic acids and carbohydrates can be trapped in a matrix of these insoluble and cross-linked proteins.[10] Partial binding of these lipids enables them to be fixed sufficiently to resist routine processing and embedding in paraffin wax.[11] This predominantly describes the plasma membrane which is a continuous double-layer of phospholipids, interweaved with cholesterol and proteins. The plasma membranes also constitute the structure of the nuclear envelope.[12] Myelin and lipofuscin are good examples whereby lipid-relaxed components can be stained in FFPE sections.[13,14] The plasma membrane also contains many lipid rafts. These rafts are known to exhibit high concentrations of sphingolipids, a type of phospholipid with long-chain saturated fatty acid tails.[15] The exact nature of the bound lipids present after the formalin fixation process has yet to be determined. Yet if these solvent-resistant, bound hydrocarbons were not removed in the solvent washing process prior to the addition of paraffin, it seems difficult to imagine by what chemical mechanism they would be leached during paraffin removal, under the same solvent conditions.

In light of this fact, the following study was performed to explore the dewaxing process issue in the context of prostate cancer tissue sections by systematic acquisition of spatially resolved infrared images by using a focal plane array (FPA) detector. By this approach, spatial information is retained and associated with the spectra throughout the classification process, presenting a more reliable way to compare tissue sections that are often heterogeneous.

2 Experimental

2.1 Reagents and materials

Paraffin wax embedded prostate cancer tissue blocks were collected under ethical approval (Trent MREC 01/4/061). The standard histological sample collection protocol involved chemical fixation of the tissue sample in 4% formalin for 24 hours. A Thermo Shandon Excelsior Processor was then used to pass varying concentrations of ethanol (20%, 90% and four aliquots of 100%) for an hour each through the tissue sample. This was followed by three, 1 hour xylene washes at 40 °C and three 1 hour washes with Paraplast at 62 °C. The tissue sample was then immersed in molten paraffin wax and cooled using an ice plate for 1 hour before the embedded tissue was storage-ready.[16]

2.2 Sample preparation

Three 4 μm serial sections were cut and two of the sections were floated onto calcium fluoride slides (1.2 mm thick, 12 mm diameter). The third section was placed on a standard histology glass slide. The glass slide specimen was then dewaxed under standard local histological protocol (5 minutes submersions in 3 different glass troughs filled with xylene). This section was then stained with Haematoxylin and Eosin (ESI, Fig. S1†).

2.3 Solvent immersion protocol

The two sections on the infrared substrates were each designated for either xylene or hexane dewaxing solvents. The solvent selection would remain constant for the specific section throughout the experiment. Both solvents were ordered from Sigma-Aldrich Co Limited (hexane, (reagent-plus >99%) Cat. 139386 and Xylene, (histological grade) Cat. 534056). Due to the toxic nature and volatility of these solvents, all dewaxing activity was carried out in a fume hood.

The protocol was kept consistent for each time point. Tissue samples were dipped 10 times (in a 20 mL beaker) holding 3 mL of the respective solvent. After the 10th dip, the sample was then left immersed within the solvent for the specified amount of time. The sample was removed and dipped 10 times (in a 20 mL beaker) holding 3 mL of ethanol and then left to air dry at room temperature for 30 minutes. After each procedure, the infrared image was acquired. For time point one, 'T1', the tissue was immersed in solvent for 5 minutes (Fig. 1, ESI, Fig. S2†). Following T1, the immersion time was increased by varying intervals up to an immersion of 24 hours (T6). Immersions times greater than 15 minutes required the beaker containing the solvent and sample to be covered with Parafilm™ to prevent any of the solvent from evaporating off prematurely. The varying times of immersion in the solvent and the notation conventions are shown in Table 1.
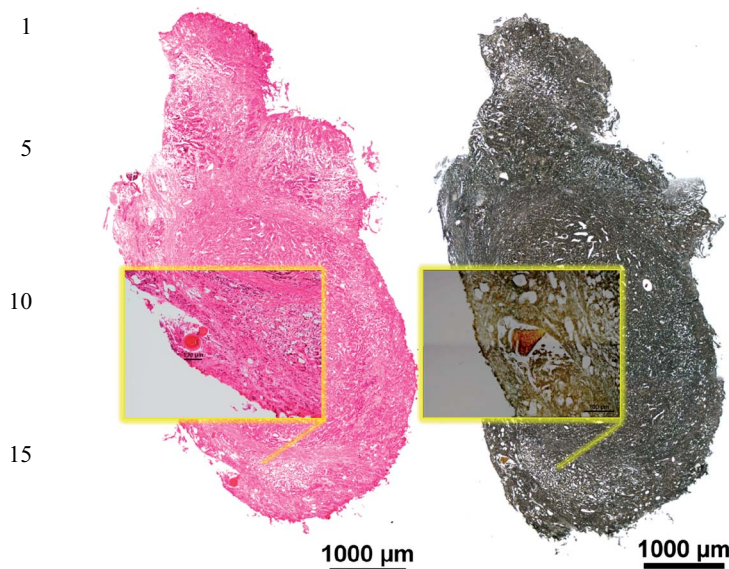
Fig. 1 Comparison between a H&E section (left) with a serial section dewaxed for 5 minutes using xylene (right). Inset: region of interest imaged during process.

Table 1 An outline of the immersion times and total sample immersion at the time of acquiring the infrared image for the region of interest

Time point	Immersion time (min)	Total time (min)
T_0	0	0
T_1	5	5
T_2	10	15
T_3	15	30
T_4	30	60
T_5	60	120
T_6	1320	1440

2.4 Data acquisition and pre-processing

Transmission mode FTIR imaging spectroscopy was performed on a Varian 670-IR spectrometer coupled with a Varian 620-IR imaging microscope (Agilent Technologies, CA) equipped with a 128 × 128 pixel liquid nitrogen-cooled Mercury–Cadmium–Telluride (MCT) focal plane array detector. Spectra were collected in the 1000–3800 cm^{-1} range, at a spectral resolution of 4 cm^{-1}, with the co-addition of 128 scans for sample spectra, and 256 scans for the background spectra. At a pixel resolution of ∼5.5 μm, a tissue sampling area of ∼700 × 700 μm was captured per hyperspectral image. Each image was subject to RMieS-EMSC correction with 20 iterations using a Matrigel™ spectrum as the initial reference point.[17,18] The infrared hyperspectral images were pre-processed according to the protocol reported in Hughes *et al.*[19] Briefly, images were quality-controlled to remove any noise-intensive signals related to non-tissue related artefacts (Fig. 2a). Remaining spectra were transformed to the first derivative before PCA was performed for each hyperspectral image, retaining the scores for 10 PCs for
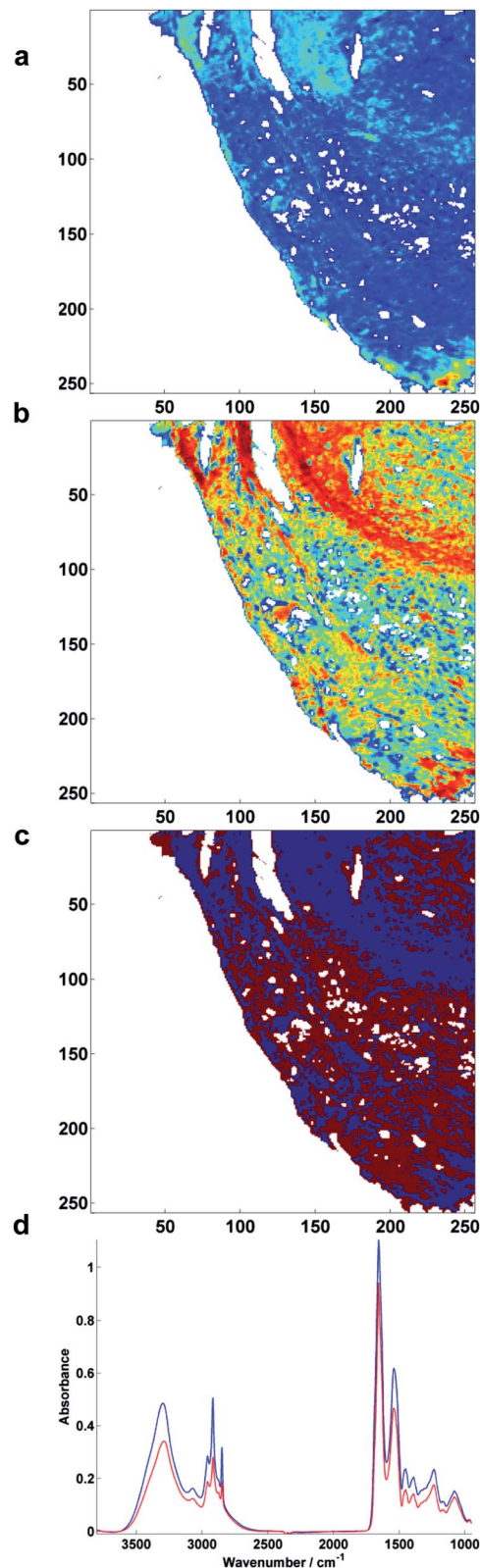

Fig. 2 Summary of the tissue classification process (a) total intensity of absorbance image after quality control to remove poorly absorbing spectra based upon an amide I threshold (b) PCA was performed to reduce dimensionality of data: PC1 suggests 2 classes of tissue present (c) *K*-means cluster analysis was performed with 2 classes on PCs 1–10 (explaining 95% of variance); (d) mean representative spectra of each extracted class where class 1 is blue and class 2 is red.
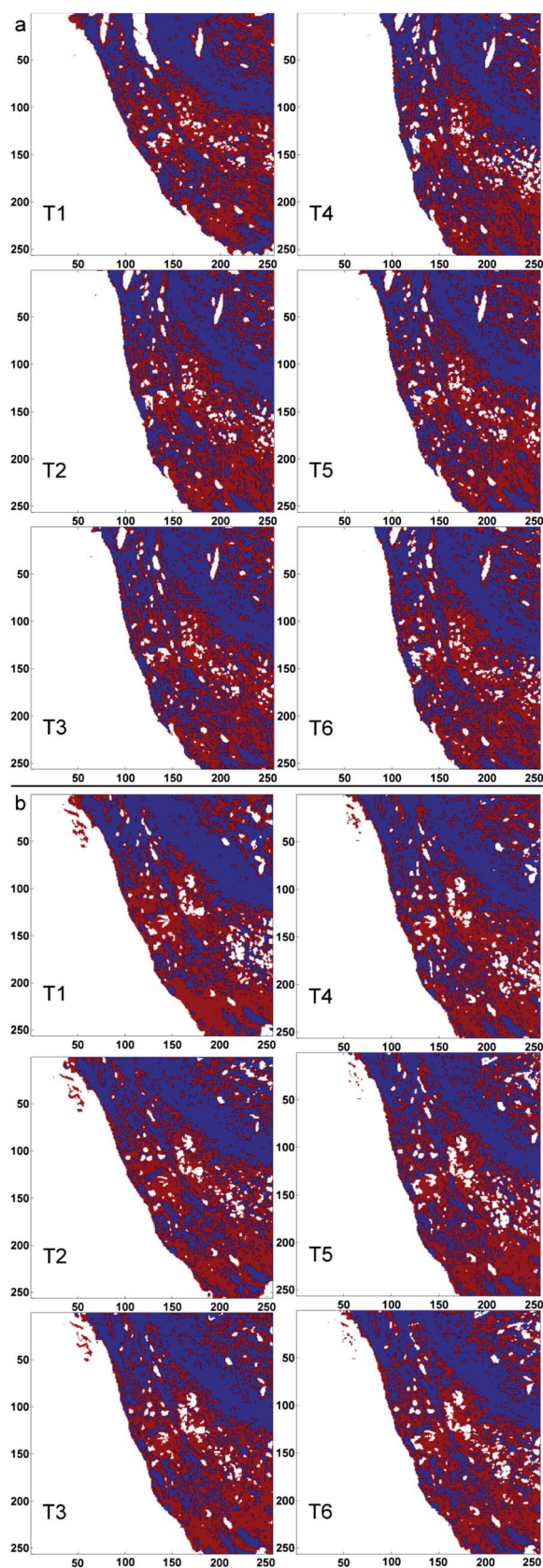
Fig. 3 Pseudo-colour K-means cluster maps describing class 1 (blue) and class 2 (red) tissue structures per time point (T1–T6) for the xylene-treated section (a) and the hexane treated section (b).

dimension reduction, corresponding to 95% explained dataset variance (Fig. 2b).

2.5 Data analysis

K-means cluster analysis was performed (with three replicates to avoid convergence of local minima) on the principal component scores using a cosine distance metric to define the image by two partitioned clusters (Fig. 2c). Subsequent pseudo-colour cluster maps were constructed, assigning a specific colour to each spectral cluster and compared to the respective H&E section for definitive histopathological evaluation (Fig. 1 and 3). The two classes (class 1, blue and class 2, red) describe different tissue structures, such as stroma (class 1) and epithelium (class 2). Using the defined cluster classes as a mask, the corresponding original spectra were extracted (Fig. 2d).

Finally, the extent of methylene bond vibrations were analysed by the calculation of two ratios (Fig. 4). These ratios were quantified in each IR image by the proportion of $\nu_{as}(CH_2)$ methylene stretching ($\sim$2917 cm^{-1}) and $\delta(CH_2)$methylene bending ($\sim$1462 cm^{-1}) peak heights, normalised over $\nu_s(OH)$ ($\sim$3289 cm^{-1}) or $\nu_{as}(PO)$($\sim$1236 cm^{-1}) peak heights (eqn (1) and (2)).

$$\text{Ratio1} \quad \frac{I\ \nu_{as}(CH_2)_{2917}}{I\ \nu_{as}(CH_2)_{2917} +\ I\ \nu_s(OH)_{3289}} \quad (1)$$

$$\text{Ratio2} \quad \frac{I\ \delta(CH_2)_{1462}}{I\ \delta(CH_2)_{1462} +\ I\ \nu_{as}(PO)_{1236}} \quad (2)$$

3 Results and discussion

The pseudo-colour classification images shown in Fig. 3 for the tissue sections immersed in either solvent for varying time periods show virtually no change as a function of time. This is important since it implies that there was no substantial difference in the wax retention from different types of tissue as classification of tissue type remained stable. The spectral signal of paraffin includes high absorptions in a number of regions of the wavenumber mid-range (ESI, Fig. S3†). If residual paraffin had been present, large differences in spectral intensities would have obscured tissue classification (ESI, Fig. 4†). This may have caused class 2 spectra to be classed as class 1 spectra, for
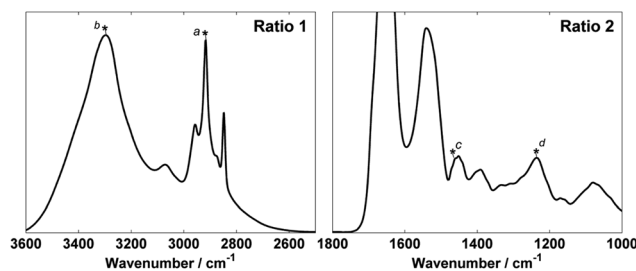

Fig. 4 Peak height ratio 1 (*a/a+b*) were $a = \nu_{as}(CH_2)$ and $b = \nu_s(OH)$ (left). Peak height ratio 2 (*c/c + d*) where $c = \delta(CH_2)$ and $d = \nu_{as}(PO)$ (right).

example and would have resulted in random classification pattern with no histological relevance.

The molecular vibrations associated with paraffin can never be unique and associated to exclusively in either Raman and IR spectra as the structural bonding present is also present in abundance in biological molecules. There is a view, however, that FTIR spectroscopy is contextually less sensitive than Raman spectroscopy for the analysis of paraffin signal contamination.[20] The basis for this viewpoint stems from comparative Raman and IR studies where investigations have been limited to the fingerprint region of the IR spectrum (800–1800 cm^{-1}).[21] There are also comparatively more assignable (sharp) peaks in the Raman spectrum of paraffin.[22] If a full-ranged mid-IR spectrum of paraffin is considered, however, there are dramatically sharp methyl and methylene-related stretching mode peaks with intensive absorbance values that extend beyond the scale of typically-prepared biological tissue (ESI, Fig. S3 and S4†). Fig. 5a displays an unprocessed single pixel spectrum from an area of tissue Sample 2 in paraffin, prior

to dewaxing. The paraffin ranged in thickness across the sample to the point of extreme saturation (ESI, Fig S4†). If the paraffin-dominated peaks present at ~1462, 2846 and 2954 cm^{-1} with absorbance values of 0.38, 1.43 and 0.54 are considered, the peaks at 2846 cm^{-1} and 2954 cm^{-1} are approximately × 3.7 and × 1.42 larger than the peak at 1462 cm^{-1}. Fig. 5b displays the mean tissue spectra for Sample 2 at T7 and after spectral processing. If, hypothetically, it was suspected that the spectrum was paraffin-contaminated due to observance of the peak at 1462 cm^{-1} (0.1 absorbance) then the values at 2846 cm^{-1} and 2954 cm^{-1} (0.13 and 0.12 respectively) should be closer to ~0.37 and 0.14, to be consistent with the approximate ratios of the paraffin, especially in terms of the proportionality of methylene stretching to bending vibrations. Thus, any major issue with residual paraffin in the tissue spectrum should be evident.

Infrared FPA imaging enables the collection of spatially-resolved spectra.[23] Not only can different tissue structures be identified by their infrared signal, large quantities of identified tissue class spectra can be extracted and used for subsequent evaluation. This is a major benefit, over single-point infrared spectroscopy, for example. For each tissue section and each time point, over 100 000 spectra were analysed by calculating the peak height ratios described in Fig. 3 (Tables 2 and 3 contain the detail). In the order of ~17 000 spectra were analysed per ratio. The ratios provided a normalised assessment of the proportion of hydrocarbon vibrations across the two tissue classes after increasing solvent immersion times.

If the solvent-action against paraffin wax was not instantaneous and ultimately stubborn to fully remove, one would expect to observe a clear, decreasing trend in the intensity of methylene bond vibrations *versus* increasing time. In reality, the actual intensity values remained fairly consistent, suggesting that the vibrations have reached a baseline level (Fig. 6). The overall %RSD values across each of the 6 time point ratios are summarised in Table 4. Despite the tissue sections being serial with slightly different images and treated with different
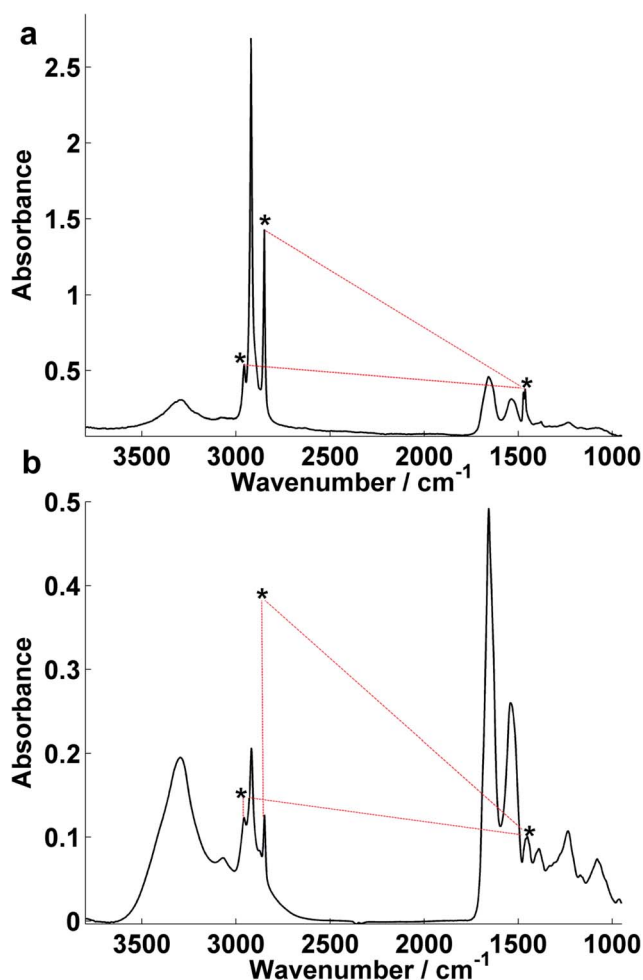

Fig. 5 A comparison between an unprocessed pixel spectrum of tissue with paraffin prior to dewaxing (a) and mean (unclassified) tissue spectrum for Sample 2 (hexane-treated) at T7 (b) (* denotes selected paraffin-related peaks at 1462, 2846 and 2954 cm^{-1}). The red lines indicate approximate positions if paraffin was present in the spectrum, according to the value at 1462 cm^{-1}.

Table 2 Summarised values for the peak height ratio calculations and subsequent barchart plots (manuscript Fig. 5a) for the xylene-washed serial section

Xylene		Ratio 1			Ratio 2		
Time point	N	$\bar{x}$	σ	% RSD	$\bar{x}$	σ	% RSD
Class 1							
T1	17 612	0.506	0.050	9.9	0.496	0.024	4.7
T2	18 128	0.503	0.052	10.4	0.498	0.022	4.3
T3	18 706	0.503	0.052	10.3	0.503	0.021	4.2
T4	17 782	0.494	0.054	10.9	0.506	0.022	4.4
T5	17 857	0.492	0.055	11.2	0.491	0.023	4.7
T6	18 159	0.504	0.053	10.4	0.504	0.022	4.4
Class 2							
T1	17 040	0.449	0.046	10.2	0.462	0.029	6.3
T2	16 721	0.461	0.042	9.2	0.461	0.027	5.8
T3	16 351	0.462	0.045	9.8	0.464	0.030	6.4
T4	16 090	0.453	0.046	10.1	0.472	0.031	6.6
T5	16 729	0.442	0.049	11.1	0.448	0.028	6.3
T6	16 508	0.460	0.044	9.6	0.465	0.028	6.1

Table 3 Summarised values for the peak height ratio calculations and subsequent barchart plots (Manuscript Fig. 5b) for the hexane-washed serial section

Hexane		Ratio 1			Ratio 2		
Time point	N	$\bar{x}$	σ	% RSD	$\bar{x}$	σ	% RSD
Class 1							
T1	18 232	0.494	0.042	8.5	0.500	0.026	5.1
T2	18 630	0.489	0.046	9.4	0.498	0.023	4.6
T3	18 237	0.479	0.049	10.3	0.496	0.022	4.4
T4	17 983	0.471	0.050	10.7	0.487	0.024	4.9
T5	17 236	0.472	0.052	11.0	0.487	0.023	4.7
T6	17 555	0.489	0.049	10.0	0.493	0.024	4.9
Class 2							
T1	17 398	0.429	0.042	9.7	0.466	0.037	7.9
T2	17 565	0.445	0.040	9.1	0.461	0.031	6.8
T3	17 694	0.432	0.044	10.2	0.457	0.029	6.3
T4	17 232	0.433	0.044	10.2	0.443	0.034	7.7
T5	17 414	0.423	0.044	10.5	0.447	0.028	6.3
T6	17 468	0.444	0.042	9.6	0.454	0.030	6.6

Table 4 The overall relative standard deviation for each tissue class for both ratios 1 and 2, expressed as a percentage

Overall % RSD	Class 1		Class 2	
	Ratio 1	Ratio 2	Ratio 1	Ratio 2
Xylene	10.5	4.5	10.0	6.2
Hexane	10.0	4.8	9.9	6.9

Fig. 6 Barcharts depicting peak ratios +/− S.D. for each solvent-treated section and the respective tissue class. Explicit values can be found in Tables 2 and 3. The overall %RSD of peak height ratios per class are shown in Table 4.

solvents, the %RSD of peak height ratios in each class are surprisingly similar.

In both serial sections, methylene vibrations were consistently more abundant in class 1 tissue spectra. For this reason, mean spectra per time point were calculated to give the best chance of a qualitative assessment of any possible observable differences (Fig. 7). The mean spectral signals of the xylene-washed tissue specimen appeared consistent. This could suggest that to a detectable limit, all of the paraffin had been removed after the first time point. In the hexane specimen, only slight observable differences were noted between time points T1 and T2 (5 and 10 minutes solvent immersion). This can be seen by the difference in peak heights between $\nu_{as}(CH_2)$ ($\sim$2917 cm^{-1}) and $\delta_s(OH)$ ($\sim$3289 cm^{-1}) visually expressed by the gradient between them, as well as a slight change in the shape of the peak shoulder of $\delta(CH_2)$ at $\sim$1462 cm^{-1}. This may be a case of detecting residual paraffin at a relatively low percentage, where differences in the smaller absorbing band at 1462 cm^{-1} are more difficult to detect due to the height of the baseline, rather than the hypothetical case shown in Fig. 5b. Nevertheless, it seems that after 10 minutes even slight changes were not detectable, indicating a steady-state in accordance to that of chemically bound tissue.

Within the limitations of this study, it may be possible that a slightly longer immersion time (approximately 5 minutes) is required with hexane to remove the paraffin by comparison with xylene. Typically the paraffin from FFPE tissue sections is removed by solvents such as xylene or hexane. Previous studies[6] have reported to monitor paraffin removal by the disappearance of the 'paraffin' band at 1462 cm^{-1} (ESI, Fig. 3†). This, however, is not a peak that is unique to paraffin as it is a bending (scissoring) vibration of methylene (CH$_2$). Biological molecules themselves will have abundant naturally-occurring methylene bending vibrations of similar strength.[24–26] A more contextual example can be seen in the spectra of human prostate cells that have been formalin-fixed (and not treated with paraffin) that evidentially display the distinct $\delta(CH_2)_{1462}$ peak shoulder.[27]

Analysis of the dewaxing efficiency of xylene with Raman spectroscopy has been reported, but with conflicting evidence. Previously, xylene has been shown to be less effective than hexane, but only by observation of selective paraffin-associated peaks.[28] One would expect to see a decreasing trend in all paraffin-associated peaks to interpret the result as a single consequence of paraffin removal. If this is not the case, it could be reasoned that there are other contributing factors involved. Changes in paraffin temperature, for example, can illicit
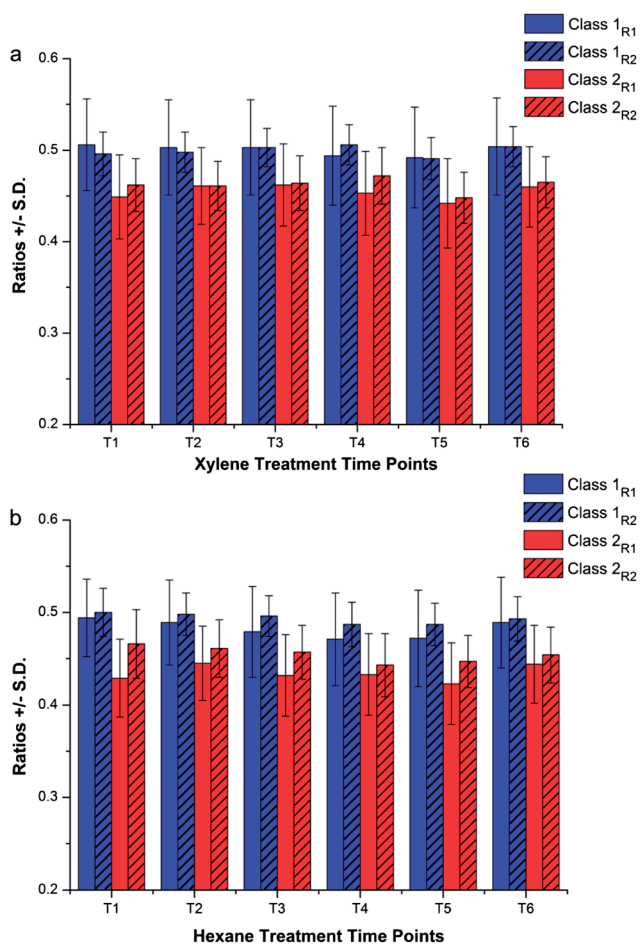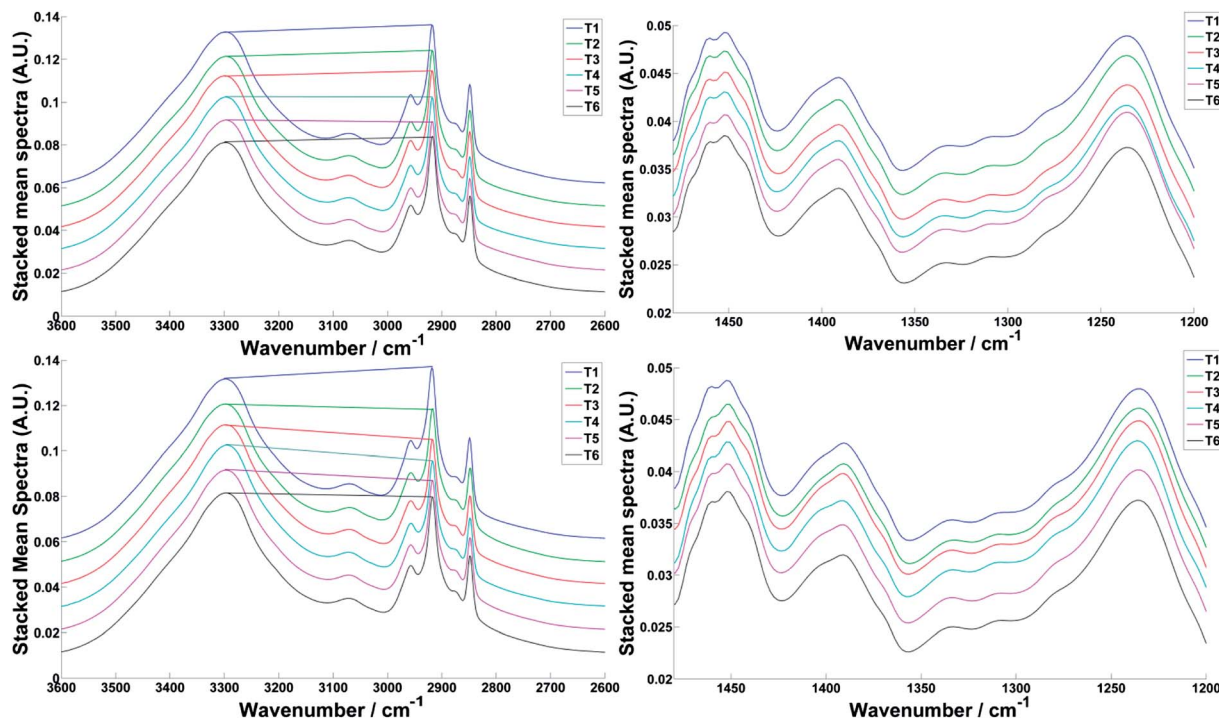
Fig. 7 Mean representative spectra calculated from the region of ~18 000 spectra per IR time-point image for class 1 tissue from the two serial sections treated with xylene (top) and hexane (below).

conformational structural modifications which can in turn cause differences in band intensity.[29] More recently, however, dewaxing of a 20 μm tissue section with xylene was reported to be effective when analysed by Raman spectroscopy,[5] which is supportive of the observations found in this study. A potential indication for the discrepancy between studies may be that the efficacy of a dewaxing protocol may differ with various tissue types. While this cannot be ruled out, the findings of this IR study of prostatic tissue that compared the results of two sub-types from a single organ (epithelial and stromal) tissue, indicated no difference in dewaxing efficacy. The only observably difference was inherent abundance of bound lipids, which remained consistent throughout the study. In the case of previous Raman studies, other possible reasons for the discrepancy could be due to differences in the protocol execution, or the fact that without spatially-resolved data analysis it is difficult to monitor the exact position of single-point data acquisition between tissue sample manipulation steps.

Most recently, a comprehensive single-point Raman study has investigated tissue of different organ type and tumour-related progression in terms of Histoclear dewaxing efficiency using a number of different substrates.[20] Interestingly, there is convincing evidence to suggest the choice of substrate may play a role in poor dewaxing which is something to equally consider for infrared experiments. Significant lipid-associated spectral differences were also found between normal and metastatic brain tumours. This evidence suggests that there are added complications when comparing tissue different sites of the body and one would have to carefully consider the differences in residual paraffin *versus* the differences related to inherent

tumour biology. For example, progression of malignant brain tumours is dependent upon vascularity and is associated with altered ganglioside composition and distribution[30] (ganglio-sides are cell surface-enriched glyco-sphingolipids) which would also cause inherent differences in lipid contributions.

4 Conclusions

In conclusion, we make the suggestion that paraffin removal by hydrocarbon solvent washing removes only those hydrocarbons present in free, unbound paraffin. The analysis of biologically native methylene vibrations should not be treated with suspicion, provided that the protocol provides evidence that paraffin is removed to the point that the methylene vibrations are at a stable baseline. A further limitation is that biochemical interpretation from such vibrations should only allude to chemically bound-lipid-complex associations. Frozen sections, however, remain the primary choice of sample preparation in order to probe the full complement of lipid structures within biological tissue.

In the confines of this experiment, we found no major difference between the use of the aliphatic hydrocarbon hexane *versus* the aromatic hydrocarbon solvent xylene. Although both solvents are particularly harmful in a health and safety context, hexane is more flammable than xylene (flash points of solvents stated in Section 2.3 are cited from their respective MSDS as −26 °C *versus* 25 °C). Therefore as a recommendation, we suggest that FFPE tissue should be de-waxed for a minimum of 5–10 minutes with xylene as it an industry standard for tissue processing. It may be advisable to adopt a more cautious

protocol; however, that given there is no evidence of tissue damage as a function of immersion time. Such a protocol could include several 5–10 minutes immersions in fresh solvent.

References

1 Y. S. Song, D. Adler, F. Xu, E. Kayaalp, A. Nureddin, R. M. Anchan, R. L. Maas and U. Demirci, *Proc. Natl. Acad. Sci. U. S. A.*, 2010, **107**, 4596–4600.

2 E. Gazi, J. Dwyer, N. P. Lockyer, J. Miyan, P. Gardner, C. Hart, M. Brown and N. W. Clarke, *Biopolymers*, 2005, **77**, 18–30.

3 D. M. Stitt, M. Z. Kastyak-Ibrahim, C. R. Liao, J. Morrison, B. C. Albensi and K. M. Gough, *Vib. Spectrosc.*, 2012, **60**, 16–22.

4 A. Tfayli, C. Gobinet, V. Vrabie, R. Huez, M. Manfait and O. Piot, *Appl. Spectrosc.*, 2009, **63**, 564–570.

5 S. M. Ali, F. Bonnier, A. Tfayli, H. Lambkin, K. Flynn, V. McDonagh, C. Healy, T. Clive Lee, F. M. Lyng and H. J. Byrne, *J. Biomed. Opt.*, 2013, **18**, 061202.

6 D. C. Fernandez, R. Bhargava, S. M. Hewitt and I. W. Levin, *Nat. Biotechnol.*, 2005, **23**, 469–474.

7 R. Chetty and S. Serra, *Am. J. Surg. Pathol.*, 2010, **34**, 401–404.

8 M. H. Ross and W. Pawlina, *Histology: a text and atlas, Adipose Tissue*, 6th edn, Lippincott Williams and Wilkins, 2010, ch. 9, p. 121.

9 V. B. Wigglesworth, *J. Cell Sci.*, 1971, **8**, 709–725.

10 S. Renshaw, in *Immunohistochemistry: Methods Express*, ed. S. Renshaw, Scion Publishing Ltd, Bloxham, UK, 2007, ch. 4, p. 50.

11 M. C. Berenbaum, *Q. J. Microsc. Sci.*, 1958, **s3–99**, 231–242.

12 G. M. Cooper, *The Nuclear Envelope and Traffic between the Nucleus and Cytoplasm*, http://www.ncbi.nlm.nih.gov/books/NBK9927/, accessed 25/07/2013.

13 P. Morell and R. H. Quarles, in *Basic Neurochemistry: Molecular, Cellular and Medical Aspects*, ed. G. J. Siegel, B. W. Agranoff and R. W. Albers, Lippincott-Raven, Philadelphia, 6th edn, 1999, ch. 4.

14 M. Mahmoodi, S. Zhang, S. Salim, J. S. Hou and F. U. Garcia, *Ann. Diagn. Pathol.*, 2006, **10**, 257–262.

15 J. P. Slotte, *Prog. Lipid Res.*, 2013, **52**, 424–437.

16 M. J. Baker, E. Gazi, M. D. Brown, J. H. Shanks, N. W. Clarke and P. Gardner, *J. Biophotonics*, 2009, **2**, 104–113.

17 P. Bassan, H. J. Byrne, F. Bonnier, J. Lee, P. Dumas and P. Gardner, *Analyst*, 2009, **134**, 1586–1593.

18 P. Bassan, A. Sachdeva, A. Kohler, C. Hughes, A. Henderson, J. Boyle, J. H. Shanks, M. Brown, N. W. Clarke and P. Gardner, *Analyst*, 2012, **137**, 1370–1377.

19 C. Hughes, J. Iqbal-Wahid, M. Brown, J. H. Shanks, A. Eustace, H. Denley, P. J. Hoskin, C. West, N. W. Clarke and P. Gardner, *J. Biophotonics*, 2013, **6**, 73–87.

20 L. M. Fullwood, D. Griffiths, K. Ashton, T. Dawson, R. W. Lea, C. Davis, F. Bonnier, H. J. Byrne and M. J. Baker, *Analyst*, 2014, **139**, 446–454.

21 E. Ó. Faoláin, M. B. Hunter, J. M. Byrne, P. Kelehan, M. McNamara, H. J. Byrne and F. M. Lyng, *Vib. Spectrosc.*, 2005, **38**, 121–127.

22 V. Vrabie, C. Gobinet, O. Piot, A. Tfayli, P. Bernard, R. Huez and M. Manfait, *Biomed Signal Process Contr*, 2007, **2**, 40–50.

23 K. M. Dorling and M. J. Baker, *Trends Biotechnol.*, 2013, **31**, 437–438.

24 R. N. A. H. Lewis and R. N. McElhaney, ed. Dopico, 2007, vol. 400, pp. 207–226.

25 C. Laugel, N. Yagoubi and A. Baillet, *Chem. Phys. Lipids*, 2005, **135**, 55–68.

26 H. S. Mansur and J. E. Oliveira, Beijing, 2007, vol. 121–123, pp. 863–866.

27 M. J. Baker, C. Clarke, D. Démoulin, J. M. Nicholson, F. M. Lyng, H. J. Byrne, C. A. Hart, M. D. Brown, N. W. Clarke and P. Gardner, *Analyst*, 2010, **135**, 887–894.

28 E. O. Faolain, M. B. Hunter, J. M. Byrne, P. Kelehan, H. A. Lambkin, H. J. Byrne and F. M. Lyng, *J. Histochem. Cytochem.*, 2005, **53**, 121–129.

29 M. Zheng and W. Du, *Vib. Spectrosc.*, 2006, **40**, 219–224.

30 T. N. Seyfried and P. Mukherjee, *J. Oncol.*, 2010.